ACS APPLIED NANO MATERIALS

www.acsanm.org

Forum Article

Cellulose Nanocrystal Composites with Enhanced Mechanical Properties for Robust Transparent Thin Films

Elena Missale, Devid Maniglio, Giorgio Speranza, Marco Frasconi, and Maria F. Pantano*

Cite This: https://doi.org/10.1021/acsanm.3c02946

Read Online

ACCESS | Metrics & More | Article Recommendations | Supporting Information

ABSTRACT: Cellulose is attracting increasing interest as a sustainable technological material, owing to its unique combination of properties, such as abundance in nature, biodegradability, nontoxicity, cost effectiveness, and good mechanical properties. Here, we developed composite thin films based on carboxymethylcellulose (CMC) reinforced with TEMPO-oxidized cellulose nanocrystals (TOCNCs). The strength and stiffness of the CMC/TOCNC nanocomposite film increased by ∼400% and ∼20%, respectively, compared to pure TOCNC films, while preserving the deformation capability of pure CMC films, the latter being less stiff, but more ductile than pure TOCNC films. We demonstrated the tunability of the CMC/TOCNC self-assembly, through Fe^{3+} complexation, resulting in transparent cross-linked nanocomposite films with enhanced strength (163.5 ± 51.3 MPa) and stiffness (Young's modulus of 14.5 ± 4.0 GPa), with no significant loss in strain at failure (2.8 ± 1.1%). Finally, as applications of newly developed films require durability in realistic operating conditions, which do not involve static forces only, we tested our films against loading−unloading cycles, demonstrating robust and stable performance. By enabling a deeper understanding of the fabrication process and mechanical properties of cellulose-based nanocomposite films, this work expands their potential applications across a broad range of fields, from environment-related processes, such as decontamination, to the biomedical field.

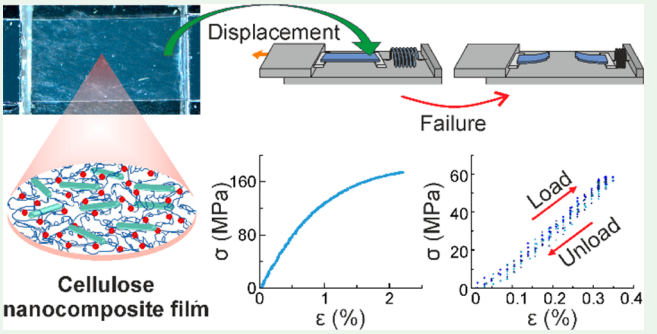

KEYWORDS: *nanocellulose, fatigue, metal-coordination, actuators, nanocomposites*

1. INTRODUCTION

The need to replace petroleum-based materials with more sustainable alternatives has become an urgent need,[1] boosting intensive research toward the development of technological solutions that take advantage of materials that are widely available in nature or can be easily derived from renewable resources.[2,3] Among these, cellulose derivatives possess an attractive combination of properties, including biodegradability and nontoxicity to humans and the environment, as well as abundance and cost effectiveness,[4] which can be exploited in a variety of applications, ranging from filtering membranes[5] to coatings and packaging,[6,7] electronic devices,[8,9] biomedical,[10,11] or energy[12,13] applications.

Cellulose can be processed via specific treatments[3] in order to derive nanomaterials with different morphologies, including short cellulose nanocrystals (CNCs) and long cellulose nanofibrils (CNFs). CNCs are rod-shaped rigid nanostructures with diameters of a few nanometers and lengths typically in the range of 100−200 nm,[14,15] while CNFs consist of both crystalline and disordered domains and have a higher aspect ratio and flexibility.[15] In particular, with regard to mechanical performance, both CNCs and CNFs possess high strength (2−6 GPa[5,16] for CNCs and 2−4 GPa[5] for CNFs) and stiffness (Young's modulus of 50−143 GPa[5,16] for CNCs and 15−150 GPa[5] for CNFs) that are comparable with those of silicon,[17,18] making them interesting candidates as structural materials for micro/nanoelectromechanical sensors as well as for soft actuators.[19,20] CNCs and CNFs can be directly processed to form films,[3] but often they are used in combination with other polymers to further enhance their performance.[21−24] For example, the addition of amorphous polysaccharides to CNC suspensions resulted in composite films with up to 40% to 60% increase in Young's modulus and strength, while preserving the chiral organization and controlled iridescence.[25] The addition of 1% weight CNCs to a gelatinized starch and polyhydroxyurethane matrix allowed the strength and Young's modulus to increase by 172% and 634%, respectively,[16] demonstrating the efficacy of CNCs as reinforcement materials.

An important aspect to consider when developing materials for sustainable applications is their durability, especially in realistic operating conditions,[1] which is the key to providing

Special Issue: Women in Nano

Received: June 28, 2023
Accepted: August 21, 2023

components with extended lifetimes. In this regard, tests involving a number of loading−unloading cycles applied to thin films or devices can provide useful information; however, the response of cellulose-based materials to cyclic loading has not been widely investigated, with more prevalence of quasi-static tests, such as tensile tests, which allow one to infer about the behavior of materials basically in ideal conditions.

Due to their high surface-to-volume ratio, cellulose nanomaterials can be chemically modified to provide surface functionalization and overcome the limits related to their hydrophilic nature, thus broadening the range of materials to which they can be combined and expanding the application possibilities.[15] In this regard, oxidation treatments, such as TEMPO-mediated oxidation (via 2,2,6,6-tetramethylpiperidin-1yl-oxyl), can be used to introduce carboxylic acid moieties in CNCs, which in turn can support additional modification by binding with different biomolecules, such as amino acids,[26] peptides,[27] or antibodies,[28] thus fostering potential biomedical applications.

In order to advance the applications of cellulose-based nanocomposite films, it is crucial to gain a comprehensive understanding of the self-assembly behavior that involves different length scales during the fabrication of the films.[29] This understanding will enable the correlation between polymer/nanofiller self-assembly and the resulting mechanical properties of the films, providing valuable information on the structure−processing−property relationship of cellulose-based nanocomposite systems that will support the development of robust devices with advanced performance.

In this study, we considered (TEMPO)-oxidized cellulose nanocrystals (TOCNCs) as reinforcement fillers added to carboxymethylcellulose (CMC) matrix to produce fully cellulose nanocomposite thin films showing remarkable load bearing and deformation capabilities, especially compared to those of films containing only their isolated building blocks (i.e., pure TOCNC and CMC films). CMC is chosen as a polymer matrix because it is expected to form compatible composite films with TOCNCs owing to their similar surface properties with carboxymethyl groups and hydroxyl groups on the cellulose chain. As one of the most widely used cellulose derivatives, CMC finds extensive applications in paper, textile, pharmaceutical, and food processing industries, where it serves as a viscosity modifier or edible coating.[30,31] Due to the good film-forming properties, CMC has been used to produce films for different applications, spanning from sensing technology[32] to food packaging.[33] In food packaging, for example, CMC-based films demonstrate outstanding features such as high optical transparency and good oxygen-barrier properties.[31,33] Despite these properties, CMC-based films exhibit limitations in terms of mechanical properties, such as strength. Therefore, to develop strong films, CMC has been combined with different cellulose nanomaterials, such as CNC or CNF, enhancing their potential applications.[31,34−36] In this regard, nanocomposite films comprising CNC mixed with CNF or CMC in different ratios have been investigated for food packaging applications.[34] In particular, the Young's modulus of the CNC/CMC nanocomposite films was found to increase with a higher proportion of CNC, reaching a maximum of ∼12.5 GPa at a content of 80% CNC. Furthermore, Aun and Rhim[37] reported on the characterization of CMC-based films reinforced with CNCs obtained from oxidation of cotton linter fibers or microcrystalline cellulose. The incorporation of oxidized CNCs led to a significant enhancement in the mechanical properties of CMC-based films, with the Young's modulus reaching up to 2.6 GPa at a CNC proportion of 10%.[37] This higher stiffness was attributed to the establishment of stronger interfacial interactions between the oxidized CNCs and the CMC polymer, induced by a large number of hydrogen bonds formed between the hydroxyl and carboxyl groups on the surfaces of CNCs. Furthermore, since multivalent metal ions (i.e., Fe^{3+}) were shown as able to induce metal−ligand coordination bond with the cellulose chain and to promote cross-linking,[38,39] we investigated the effect of Fe^{3+} ions on the mechanical properties of our nanocomposite cellulose films. In particular, we have recently found that the formation of strong metal-cross-linked cellulose networks is attributed to the combination of ionic coordination bonds between the negatively charged carboxylate groups of CMC[39] or TOCNC[40] and Fe^{3+} cations, as well as the glucopyranose sugar ring−Fe^{3+} interactions. These interactions involving Fe^{3+} play a crucial role in stabilizing and strengthening the cellulose matrix. Furthermore, due to the interconversion between Fe^{3+} and Fe^{2+} ions, cross-linking by iron can also be used to induce redox- and photoresponsive cellulose-based materials and expand their potential applications, such as photocatalytic degradation of organic pollutants.[41] In the present study, we demonstrated that the self-assembly of cellulose composite films and their macroscopic properties can be tuned by varying the concentration of Fe^{3+} ions which, at low concentration, can be an effective route for improving both the strength and stiffness of the cellulose films. Finally, to achieve a deeper insight into the possibility of using the developed films in realistic device applications, we also assessed their performance under cyclic loading, which revealed robust and stable behavior. These findings lay the foundation for unlocking the full potential of cellulose-based nanocomposite films that will enable their applications to expand across a broad range of fields, encompassing decontamination, catalysis, and even the realm of soft actuators.

2. EXPERIMENTAL SECTION

Materials. TOCNC 1 wt % dispersion with a degree of oxidation of ca.1.0 mmol/g was provided by CelluloseLab (Canada). The TOCNC nanorod dimensions were 8−15 nm in width and 100−150 nm in length. Sodium carboxymethyl cellulose (NaCMC; MW = 250 kDa) with a degree of substitution (DS) of 0.9 and iron(III) nitrate nonahydrate [$Fe(NO_3)_3{\cdot}9H_2O$; 98%] were purchased from Sigma-Aldrich Co. (St. Louis, MO).

Thin Film Preparation. TOCNC and CMC dispersions at 0.2 wt % were prepared by dilution from 1 wt % stock dispersions of TOCNC and CMC. The 1:1 mixture of CMC and TOCNC dispersion was prepared by slowly adding a 0.2 wt % dispersion of TOCNC to a 0.2 wt % of CMC under vigorous stirring, followed by ultrasonication for 10 min to prevent aggregation of the mixture. The (CMC/TOCNC)−Fe^{3+} dispersions were prepared by adding a Fe^{3+} stock solution (10 mM from $Fe(NO_3)_3{\cdot}9H_2O$) to the CMC/TOCNC mixture to achieve the final Fe^{3+} concentrations of 0.2 mM (low), 0.7 mM (medium), and 1.2 mM (high). To avoid aggregation of the suspension by the addition of Fe^{3+} ions, the samples were kept under continuous stirring conditions. Thin films were prepared by pouring the dispersions into a glass dish and air drying for 6 days. The six resulting thin transparent cellulose-based films were labeled as CMC, TOCNC, CMC/TOCNC, (CMC/TOCNC)Fe-low, (CMC/TOCNC)Fe-med, and (CMC/TOCNC)Fe-high. The thickness of the films was measured using an IMS-5s measuring probe supplied by IBR Messtechnik GmbH & Co. KG. The thickness of each film was averaged over five values.

https://doi.org/10.1021/acsanm.3c02946
ACS Appl. Nano Mater. XXXX, XXX, XXX−XXX

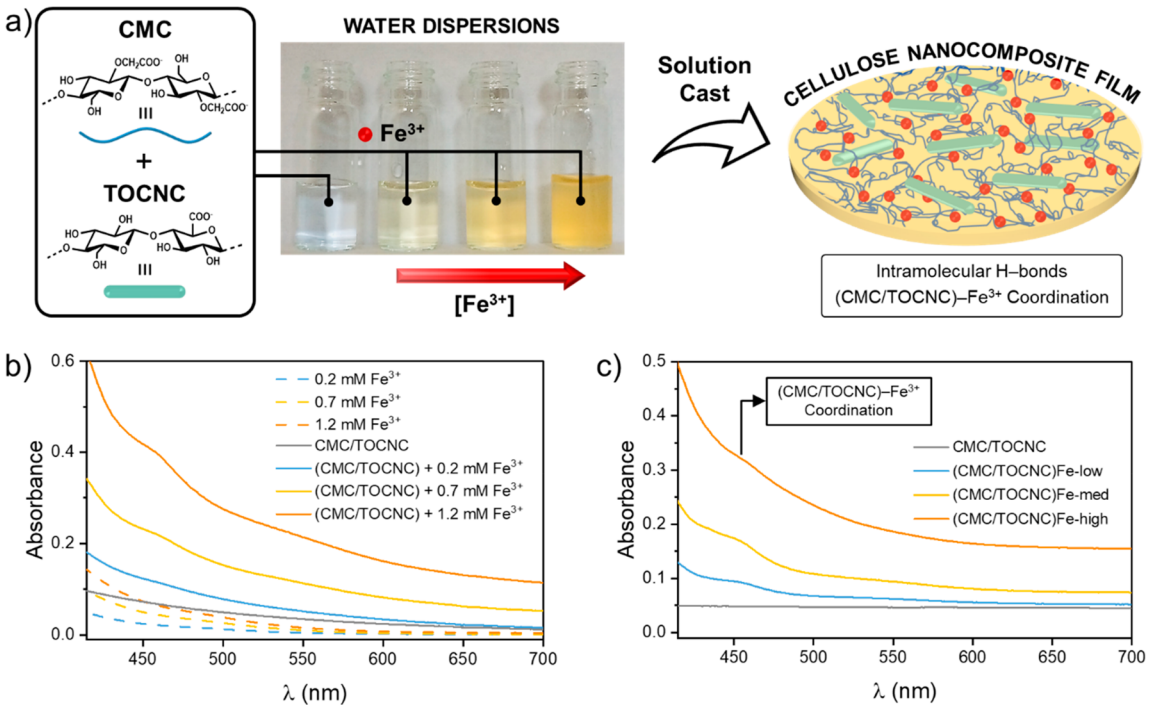

Figure 1. (a) Chemical structure of the repeating unit of carboxymethyl cellulose (CMC) and TEMPO-oxidized cellulose nanocrystals (TOCNCs), along with the schematic representation of the film preparation and of the CMC/TOCNC nanocomposite cellulose film cross-linked by Fe^{3+} ions. Images of water suspensions of CMC/TOCNC in the absence and in the presence of Fe^{3+} ions at increasing concentrations used to obtain films by a casting method. UV−vis spectra of (b) water dispersions and (c) dried films of CMC/TOCNC in the absence and in the presence of Fe^{3+} ions at increasing concentrations. Note the absence of the absorption band around 458 nm in the case of water solution of Fe^{3+} ions (dashed lines).

UV/Vis Absorption Spectroscopy. UV/vis absorption spectra of solutions and films were recorded using a Cary 60 Agilent spectrophotometer. The transparency of the films was determined by measuring the percent transmittance of light at 660 nm (T_{660}) using the same spectrophotometer.

Zeta Potential. Zeta potential measurements of TOCNC water dispersions at 0.2 wt % were performed on a ZetaSizer NanoS system (Malvern) at 25 °C.

X-ray Photoelectron Spectroscopy (XPS). XPS was used to determine the chemical composition of the cellulose-based films. Spectra were collected using an Axis DLD Ultra spectrometer (Kratos, Manchester UK) in a wide 1300 to 0 eV binding energy (BE) range with a pass energy of 160 eV. Single core-lines were acquired in high energy resolution setting the pass energy at 20 eV and the energy at 0.05 eV. Acquisition of spectra required charge compensation. Flood gun operating conditions were established by maximizing peak intensities while reducing their full width at half-maximum (fwhm). The final energy resolution achieved using these experimental conditions was ∼0.30 eV. Finally, the spectra were deconvoluted and analyzed with a homemade software based on R platform.[42]

Scanning Electron Microscopy (SEM). SEM images were taken with a Zeiss Supra 40 microscope. Before SEM analysis, the film samples were coated with a thin gold/palladium layer. The cross-section images were obtained from film failure under tensile load.

Energy-Dispersive X-ray Spectroscopy (EDS). EDS analysis was carried out with a Bruker Quantax analyzer supplied with an XFlash 630 M detector, installed inside a JEOL IT300 SEM.

Atomic Force Microscopy (AFM). The surface topography of the developed films was studied using an NT-MDT Solver Pro system equipped with a Nova scanner. The samples were imaged in semicontact mode using silicon tips (NSG11, NT-MDT, 10 nm nominal tip radius, resonance frequency of 181 kHz), collecting 10 × 10 μm^2, 512 points resolution topography images. AFM data were analyzed with support from Gwyddion analysis software.[43] The roughness was estimated over an area of 5 × 5 μm^2. In order to reconstruct the sample topography under longitudinal deformation, the samples were glued to two pieces of silicon spaced by ∼4 mm. One silicon piece was kept fixed, while the other one was glued to a linear stage. Different images of the sample were acquired at different positions of the linear stage in order to collect the topography of the specimen with increasing applied strain.

Mechanical Characterization. Both quasi-static tensile and cyclic tests were carried out by means of a custom-made platform hosting a piezoelectric linear stage to apply unidirectional displacement and a spring with calibrated stiffness, as previously reported by us.[44,45] The spring was engraved from a 1 mm thick PVC foil and used as a load sensor. Both the linear stage and the load sensor were glued to a rectangular silicon piece. Rectangular specimens with a width of ∼3 mm and a length of ∼10 mm were cut from the prepared cellulose-based films. Before the test, each specimen was positioned to bridge the gap between the two rectangular silicon pieces of the testing platform and then glued on each side. The distance between the two pieces of silicon corresponded to the gauge length of the specimen which was kept at ∼6 mm. During the tensile test, the linear stage applies a controlled displacement at the end of the specimen connected to it, which in turn transfers part of the displacement to the load sensor spring, which, as a consequence, deforms. The tensile testing platform operates under an optical microscope that allows us to record images of the specimen deformation during the test. Images were taken at a frequency of 15 frames per second. At the end of the test, all images are elaborated using a routine implemented in Matlab software, to quantify the displacement of the specimen on both the sensor and actuator side. The strain was calculated as the ratio between the difference in displacement on the actuator and sensor side over the specimen gauge length, while the stress was calculated by dividing the force measured with the load sensor (i.e., its spring constant multiplied by its deformation) by the cross-section of the specimen (i.e., product between width and thickness). The Young's modulus was derived as the slope of the stress−strain curve in its initial region. The values of the mechanical properties derived from

https://doi.org/10.1021/acsanm.3c02946
ACS Appl. Nano Mater. XXXX, XXX, XXX−XXX

the tensile tests were obtained from the average of at least five samples. The tensile testing platform mentioned above was also used to apply loading−unloading cycles to our cellulose nanocomposite films. The values of the mechanical properties derived from tensile tests on films previously subjected to cyclic loading were obtained from the average of at least three samples.

3. RESULTS AND DISCUSSION

TOCNC colloidal particles are negatively charged in aqueous solutions with a zeta potential for TOCNC dispersions of −38 ± 3 mV, in accordance with other CNC dispersions with carboxylic surface groups reported in the literature.[46] The anionic carboxylic groups on the TOCNC surface and on the backbone of the CMC polymer can be used to manipulate the self-assembly of CMC/TOCNC composites by the formation of metal-coordination bonds in addition to hydrogen bonding interactions between the cellulose chains. As depicted in Figure 1a, our procedure starts with the preparation of a dispersion of CMC and TOCNC in a 1:1 ratio, followed by the addition of different concentrations of Fe^{3+} ions. The ratio of our CMC/TOCNC nanocomposites was set at 1:1 in order to achieve a homogeneous cross-linked network of CMC chains with TOCNC through Fe^{3+} ions. The formation of metal-coordination bonds between the CMC/TOCNC and Fe^{3+} ions is evidenced by the UV−vis spectra (Figure 1b,c), which show an absorption band at around 458 nm, characteristic of the coordination of ferric ions with carboxylic groups. On the contrary, the UV−vis spectra of solutions of Fe^{3+} ions in water show only weak absorption in the 400−500 nm range. By increasing the concentration of Fe^{3+} ions from 0.2 mM to 1.2 mM, the formation of a turbid suspension was observed (Figure 1a), which also results in an increasing offset of the UV−vis spectra, a phenomenon that can be attributed as a consequence of the formation of clusters of metal-cross-linked CMC/TOCNC. Therefore, the Fe^{3+} concentration of 1.2 mM was set as the maximum for film preparation to maintain the solution in a "gelling process" state and to avoid the formation of a gel or the precipitation of TOCNC agglomerates, which could have detrimental effects on the formation of homogeneous films.

Cellulose derivative films were prepared by casting the aqueous suspensions of pure CMC and TOCNC or their 1:1 mixture in the absence and the presence of Fe^{3+} ions at 0.2, 0.7, or 1.2 mM in a glass dish. Evaporation of the solvent at room temperature led to the formation of robust films. The CMC/TOCNC nanocomposite film revealed high transmittance against visible light, reaching a T_{660} of approximately 89%. This value is only slightly lower than the transmittance obtained for the pure CMC film (T_{660} of 91%), confirming the effective dispersion of TOCNCs within the CMC polymer, even at a 1:1 mixing ratio, without any observable agglomeration (see also optical images, Figure S1). This result is consistent with the light transmittance observed for other nanocomposite films formed by mixing CMC and CNF.[47] On the contrary, the film obtained from pure TOCNC presents a lower light transmittance (72%), in addition to strong iridescence as a result of the cholesteric nematic phase transition. The presence of Fe^{3+} ions in the nanocomposite films led to a change in the film color to yellow and the appearance of the characteristic absorption peak at approximately 453 nm (Figure 1c), indicating the formation of the coordination complex involving Fe^{3+} ions and the CMC/TOCNC system. It is interesting to note that the (CMC/TOCNC)Fe-low nanocomposite film, with a T_{660} value of 88%, maintains the excellent light transmittance property found for the CMC/TOCNC film. This result suggests that the cross-linking by Fe^{3+} ions does not result in aggregation of TOCNC, which would hinder the transmission of light through the film. However, as the amount of Fe^{3+} ions in the films increases, (CMC/TOCNC)Fe-med and (CMC/TOCNC)Fe-high, the light transmittances of the films decrease to 84% and 62%, respectively. Interestingly, a significant broadening of the absorption peak is also observed for these films (Figure 1c), which could be attributed to the larger distribution of coordination complexes originated at high Fe^{3+} concentration with the formation of small TOCNC agglomerates, partially hindering light passage through the film.

In order to shed more light on the interactions between Fe^{3+} ions and the cellulose derivatives, and quantify the formation of the (CMC/TOCNC)−Fe^{3+} complex on the surface of the different nanocomposite films, we performed X-ray photoelectron spectroscopy (XPS) analysis. The XPS survey spectrum of the nanocomposite CMC/TOCNC film shows the characteristic C and O peaks at ∼287 eV and ∼533 eV (Figure S2), respectively, while the spectra of the nanocomposite films in the presence of Fe^{3+} ions show also the peak of iron at ∼712 eV (Figure S2e,f). The fitting of the O 1s spectra of CMC/TOCNC shows (Figure 2a) three components at 531.5, 533.2, and 534.0 eV, which correspond to an oxygen atom linked by a double bond to a carbon atom (C═O), an oxygen atom linked to a carbon atom by a single bond (C−O−H), and one carbon atom bonded to two oxygen atoms (O−C−O), respectively. An additional peak at 530 eV was obtained for the nanocomposite films in the presence of iron (Figure 2b,c), which can be attributed to the formation of Fe−O coordination bond. The intensity of this component increased with the Fe^{3+} content in the films, and it was found to be about four times higher in the (CMC/TOCNC)Fe-high film compared to the (CMC/TOCNC)Fe-low film, suggesting a higher amount of coordination complexes in the (CMC/TOCNC)Fe-high system. Deconvolution of the high-resolution scans of the XPS spectra of C 1s for the CMC/TOCNC in the absence and with Fe^{3+} ions (Figure S2a,b,c), reveals the presence of four peaks at 285, 286.7, 288.5, and ∼289 eV, corresponding to (C−C/C−H), (C−O), (C═O, O−C−O), and (O═C−O), respectively, which are in agreement with previously reported XPS spectra of TOCNCs and cellulose derivatives.[48] High-resolution scans of the XPS spectra of Fe 2p revealed the characteristic peak at 712 eV for the films containing iron. The (CMC/TOCNC)Fe-high film exhibited an additional peak at 707 eV, indicating the presence of a small amount of iron aggregates in the sample (Figure S 2f).

To gain a deeper understanding of the influence of mixing CMC and TOCNC in the presence and absence of Fe^{3+} ions on the morphology and microstructure of the films, SEM images of all fabricated cellulose-based thin films have been acquired (Figure 3 and Figure S3 for higher magnification images).

The cross-section of pure TOCNC films (Figure 3a) shows a submicrometer layered texture, as also previously observed for CNC thin films,[25] which is not present in pure CMC films (Figure 3b). Layered domains extending over relatively large areas become more evident in CMC/TOCNC composite films (Figure 3c), which show only occasional defects and no evidence of phase separations. The observed homogeneous integration of rigid TOCNCs with a flexible CMC matrix can be ascribed to the formation of hydrogen bonds between the

https://doi.org/10.1021/acsanm.3c02946
ACS Appl. Nano Mater. XXXX, XXX, XXX−XXX

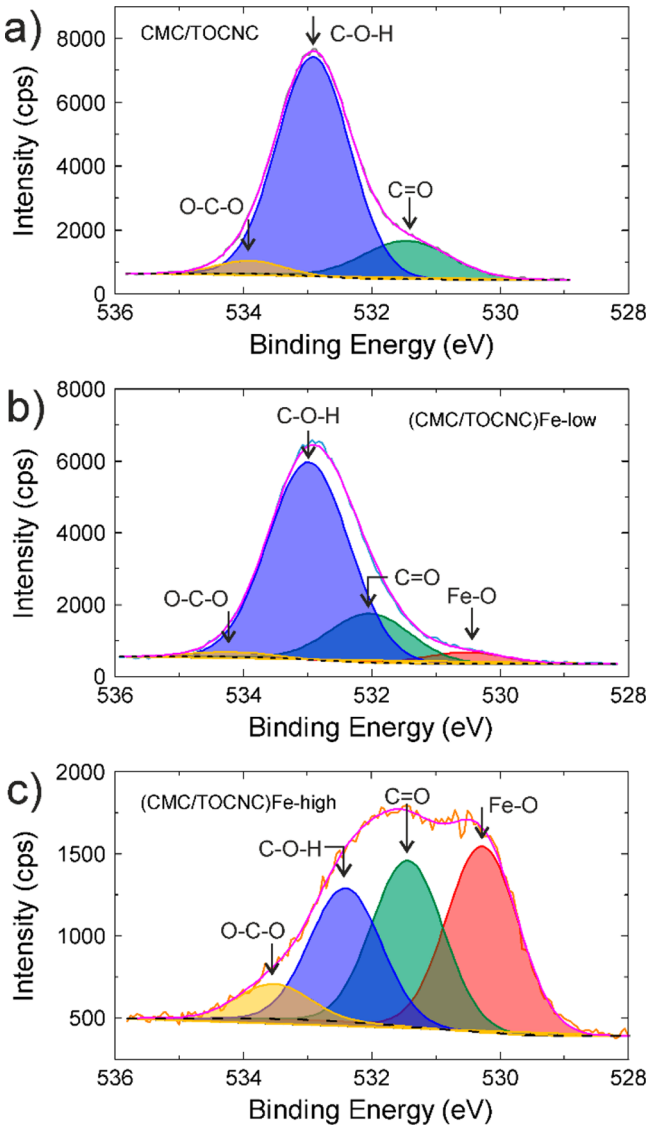

Figure 2. XPS O 1s narrow scan for (a) CMC/TOCNC, (b) (CMC/TOCNC)Fe-low, and (c) (CMC/TOCNC)Fe-high films.

OH groups of the cellulose moieties. The addition of Fe^{3+} ions further improves uniformity and compactness of the CMC/TOCNC nanocomposite films, especially at low concentrations (Figure 3d,e). At higher concentration, although Fe^{3+} content continues to be well distributed in the films, as evident from the EDS analysis (Figure 3h,j), the layered structure is partially lost with inhomogeneities and agglomerates that begin to appear on the surface (Figure 3i).

Regarding the topography, AFM analysis revealed that our CMC/TOCNC composite films possess very smooth surfaces, characterized by a roughness of about 8.5 nm. We further investigated the morphology of the produced nanocomposite films to capture eventual modification as a result of the application of a mechanical deformation. To this end, we adopted a custom-made tensile testing platform,[44,45] which we further developed in order to achieve full compatibility with the AFM scanner (Figure 4a). This allowed us to monitor the evolution of the surface topography of the film while this was subjected to a uniaxial strain. We could clearly observe the flattening of the random waviness as the applied strain increased, with no occurrence of structural distortion or modification that could trigger failure. For example, Figure 4b,c shows the surface topography of a 5 × 5 μm^2 area of a CMC/TOCNC nanocomposite film both at rest and under 0.7% longitudinal strain.

We pursued a bioinspired strategy to develop cellulose-based thin films capable of combining load-bearing and deformation capabilities. To this aim, we developed cross-linked nanocomposites films starting from a soft polymeric matrix of CMC, which we reinforced with TOCNCs to take advantage of their superior strength and stiffness. A direct comparison of the mechanical properties of pure TOCNC, pure CMC, and nanocomposite CMC/TOCNC films is reported in Figure 5, with all values collected in Table 1. The mechanical properties were derived from tensile tests carried out through the custom-made platform shown in Figure S4. Figure S5 shows the stress−strain curves obtained from all tested samples.

Pure TOCNC films result in them being relatively stiff but very brittle, especially when compared with pure CMC films. The brittleness of CNC-based films was also previously reported in the literature[35] and can be ascribed to the tendency of cellulose nanocrystal suspensions to form clusters other than interconnected flexible networks.[49] Interestingly, the addition of TOCNCs to CMC produces nanocomposite films with significantly improved mechanical properties, not only in terms of strength (145.8 ± 19.4 MPa vs 74.0 ± 10.8 MPa for pure CMC films) and Young's modulus (11.4 ± 3.1 GPa vs 4.9 ± 0.9 GPa for pure CMC films) but also toughness (4.0 ± 2.1 $MJ \cdot m^{-3}$ vs 1.8 ± 2.1 $MJ \cdot m^{-3}$ for CMC films). Although strength and toughness are usually at odds with each other,[50] in the case of our composite films, the presence of TOCNCs allows them to withstand more load but not at the expense of the deformation capability characterizing the CMC matrix, which is basically preserved. This result demonstrates that an efficient stress transfer mechanism is achieved from the matrix to the nanocrystal reinforcements, favored by the hydrogen bonds that are established between them. A synergistic action between the hard and soft phases is a typical feature characterizing natural structural materials, such as bone and nacre, but it is challenging to be replicated in biomimetic materials.[51]

The values of both strength and Young's modulus of our nanocomposite films compare favorably with those of transparent commercial polymers, such as biaxially oriented polyethylene terephthalate (Young's modulus of 4.9−5.1 GPa, strength of 200−240 MPa[52]), as well as other nanocellulose-based films reported in the literature. For example, pure CMC films with 40−50 μm thickness were reported with comparable strength (82 ± 7.5 MPa[35]) and Young's modulus of (2.5 ± 0.5 GPa[35]) yet with higher strain at failure (15 ± 3%[35]). Our CMC/TONC films show both higher strength and stiffness than CMC films with aligned CNCs reported in the literature (strength of 103 ± 10 MPa and Young's modulus of 6.5 ± 0.5 GPa[35]) yet less deformation capability (7.0 ± 2%[35]). However, in comparison to these, our films possess a similar amount of cellulose nanocrystals, although TEMPO-oxidized. With respect to other previously reported CNC/CMC composite films at 50% CNC content,[34] our films exhibit significantly higher strength and Young's modulus, as well as higher strain at failure, which can be attributed to the formation of an extensive hydrogen bond network arising from the hydroxyl and carboxyl groups on the surfaces of TOCNCs. Compared to other oxidized nanocellulose-based materials, nanocomposite films prepared by

https://doi.org/10.1021/acsanm.3c02946
ACS Appl. Nano Mater. XXXX, XXX, XXX−XXX

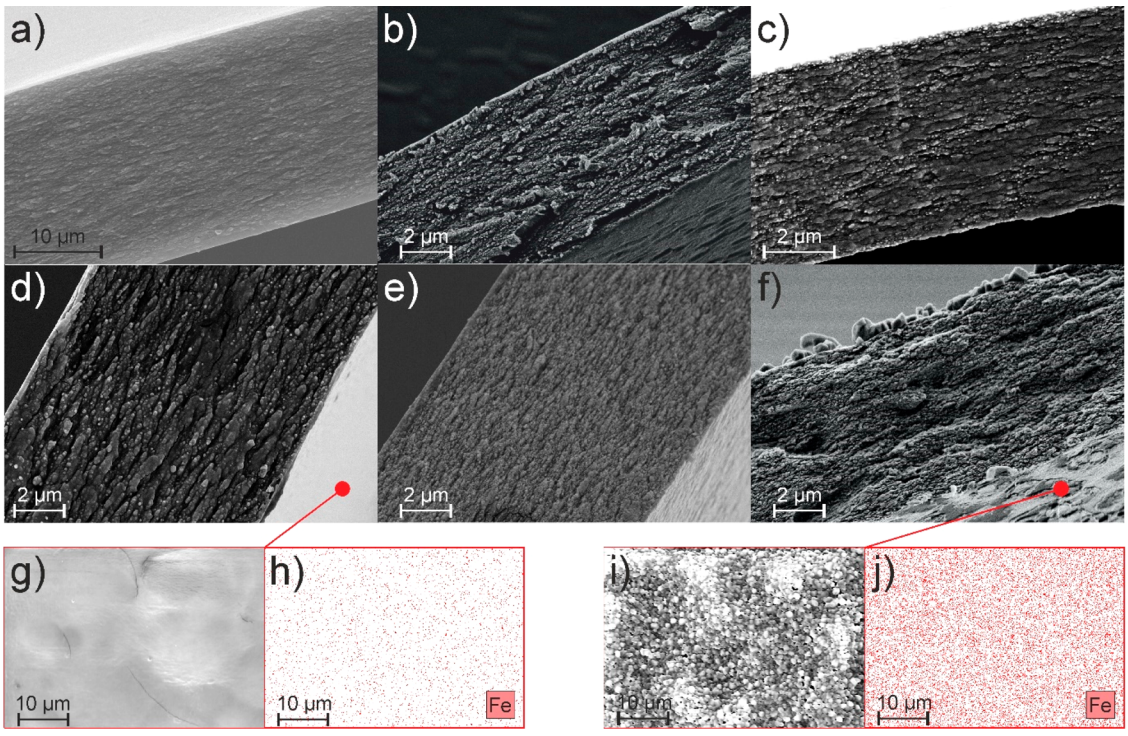

Figure 3. SEM images showing the cross-section of cellulose-based thin films. (a) Pure TOCNC film, (b) pure CMC film, (c) CMC/TOCNC nanocomposite film, (d) (CMC/TOCNC)Fe-low nanocomposite film, (e) (CMC/TOCNC)Fe-med nanocomposite film, and (f) (CMC/TOCNC)Fe-high nanocomposite film. (g) SEM image of the top view of (CMC/TOCNC)Fe-low revealing a smooth surface and (h) the corresponding EDS map indicating localized elemental presence of Fe, which appears evenly distributed. (i) SEM image of the top view of (CMC/TOCNC)Fe-high revealing superficial inhomogeneities and (j) the corresponding EDS map of Fe.

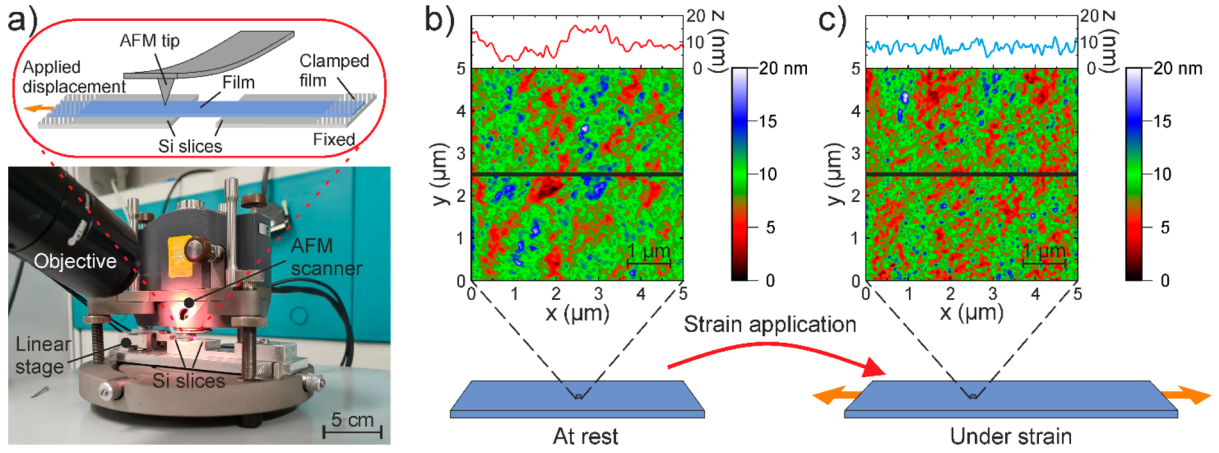

Figure 4. AFM analysis of the CMC/TOCNC nanocomposite film under strain. (a) Image and schematic representation of a custom-made setup comprising a linear stage and an AFM probe adopted to perform an AFM scan of the film during the application of a mechanical deformation. Topography of the film (b) at rest and (c) under 0.7% applied strain.

mixing CMC with 10% CNC, isolated from cotton linter using an ammonium persulfate oxidation method, exhibited lower strength (81.5 ± 3.6 MPa) and Young's modulus (2637 ± 59 MPa). On the other hand, TEMPO−CNF films with ∼30 μm thickness showed higher strength and Young's modulus (325 MPa and 20.5 GPa, respectively[52]) than our films, owing to the intrinsic good mechanical properties of CNF, but lower strain at failure (2.25%[52]).

An interesting method to tune the mechanical and rheological properties of nanocellulose-based materials uses the incorporation of ions.[53,54] In the case of our films (Table 1), at low concentration, the addition of Fe^{3+} ions is accompanied by an increase in strength (163.5 ± 51.3 MPa) and Young's modulus (14.5 ± 4.0 GPa) by ∼12% and 27%, respectively, with no significant loss of ductility (the strain at failure reduces to 2.8 ± 1.1%). This improved mechanical performance can be ascribed to the formation of strong coordinate bonds between metal ions and negatively charged carboxylate groups of the cellulose chains, which in turn promote cross-linking.[38] Investigations on wet cellulose nanofibril (CNF) films allowed identifying different mechanisms that contribute to the enhanced attractive interaction between nanocellulose structures in the presence of multivalent ions, such as ion−ion correlation, dispersion inter-

https://doi.org/10.1021/acsanm.3c02946
ACS Appl. Nano Mater. XXXX, XXX, XXX−XXX

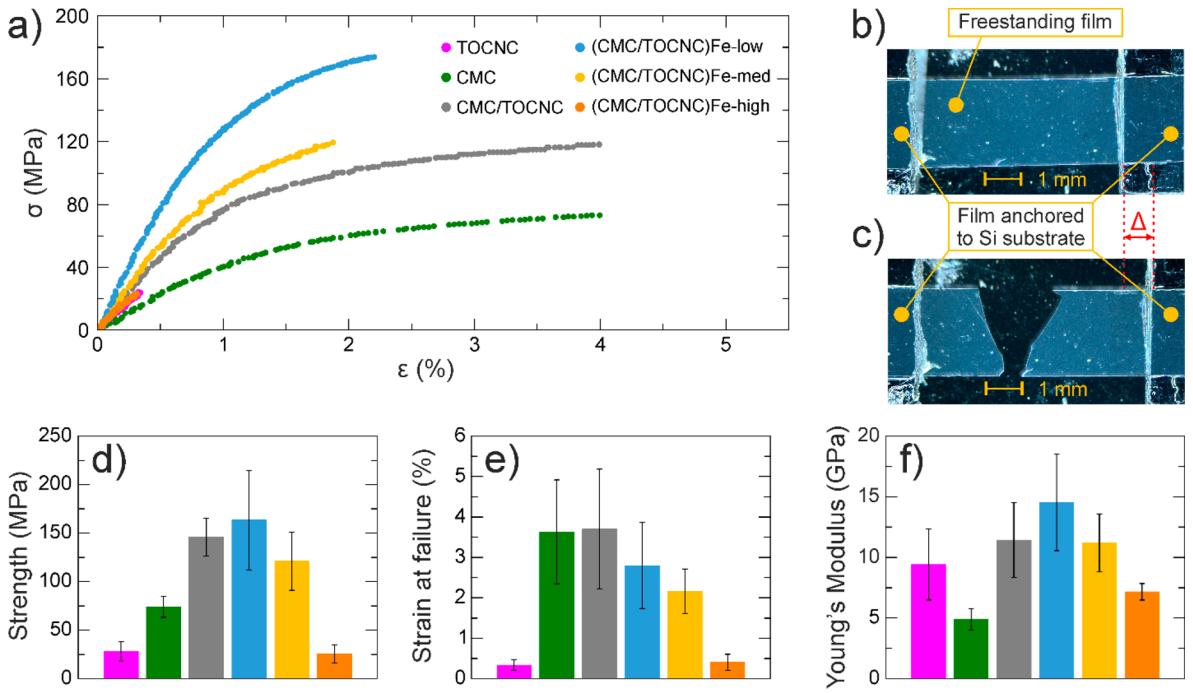

Figure 5. Mechanical characterization of cellulose-based thin films. (a) Example stress–strain curves derived from tensile tests; optical images of (CMC/TOCNC)Fe-med film sample (b) before and (c) after application of a longitudinal displacement (Δ) that caused film failure. Mechanical properties of the investigated films: (d) strength, (e) strain at failure, and (f) Young's modulus.

Table 1. Mechanical Properties of Different Cellulose-Based Films

films	thickness (μm)	tensile strength (MPa)	strain at failure (%)	Young's modulus (GPa)
TOCNC	5.5 ± 2.2	28.2 ± 9.9	0.3 ± 0.1	9.4 ± 2.9
CMC	8.6 ± 2.2	74.0 ± 10.8	3.6 ± 1.3	4.9 ± 0.9
CMC/TOCNC	7.3 ± 0.8	145.8 ± 19.4	3.7 ± 1.5	11.4 ± 3.1
(CMC/TOCNC)Fe-low	9.9 ± 2.1	163.5 ± 51.3	2.8 ± 1.1	14.5 ± 4.0
(CMC/TOCNC)Fe-med	12.7 ± 2.3	121.0 ± 30.0	2.2 ± 0.6	11.2 ± 2.4
(CMC/TOCNC)Fe-high	10.1 ± 1.7	25.6 ± 9.5	0.4 ± 0.2	7.2 ± 0.7

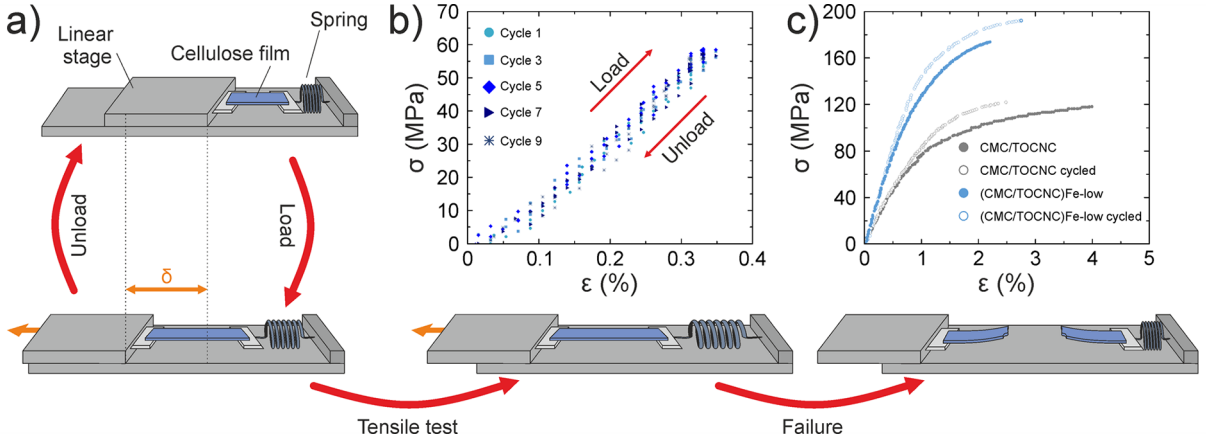

Figure 6. Mechanical behavior of cellulose nanocomposite films under and after cyclic tensile tests. (a) Schematic of the load-unload testing configuration that involved the cyclic application of a longitudinal displacement δ to a cellulose-based film specimen. Examples of (b) hysteresis curves of a (CMC/TOCNC)Fe-low film and (c) stress–strain curves of composite CMC/TOCNC and (CMC/TOCNC)Fe-low films showing that mechanical performance is not affected by the application of 20 cycles of tensile load.

actions, local metal–ligand complexes, together with a local acid environment.[55] More in detail, the robust complexation between TOCNC and Fe^{3+} ions arises from the specific interaction between Fe^{3+} ions and surface-exposed carboxylic groups of TOCNC complemented by a cooperative effect of the surrounding hydroxyl groups in the coordination.[40] The beneficial effect due to Fe^{3+} ions is however lost at higher concentration, where the addition of metal ions causes the formation of agglomerates and inhomogeneities (as visible from the SEM image of Figure 3f,i) that are detrimental for

https://doi.org/10.1021/acsanm.3c02946
ACS Appl. Nano Mater. XXXX, XXX, XXX–XXX

both the load standing and the deformation capabilities of the films.

In perspective device applications, it is important to investigate the capability of materials to maintain their mechanical performance even after loading−unloading cycles. To this end, we tested our best performing samples, i.e., CMC/TOCNC and (CMC/TOCNC)Fe-low, through cyclic tensile tests (Figure 6a). We applied a cyclic longitudinal strain value close to the end of the linear elastic regime (∼0.4%). The behavior of the films in both the loading and unloading phases overlaps throughout the cycles, without evidence of hysteresis (Figure 6b and Figure S6). In order to confirm that cyclic loads did not affect the mechanical properties of the films, we then subjected these to a tensile test. By comparing the stress−strain curves (Figure 6c and Figure S7) of such films (empty circles) with those obtained from films subjected to a single tensile test (solid circles), no significant differences can be noticed. Additionally, the corresponding values of strength (122.3 ± 27.7 MPa for CMC/TOCNC and 193.7 ± 10.3 MPa for (CMC/TOCNC)Fe-low), Young's modulus (11.9 ± 3.2 GPa for CMC/TOCNC 15.6 ± 5.2 GPa and for (CMC/TOCNC)Fe-low), and strain failure (2.1 ± 0.9% for CMC/TOCNC and 3.2 ± 0.6% for (CMC/TOCNC)Fe-low) align well with those reported in Table 1.

CONCLUSIONS

The development of sustainable devices encompasses a variety of aspects, including novel and more efficient designs able to fully exploit the properties of the material, as well as the implementation of materials provided with a lower environmental impact but good mechanical performance and robustness also in nonideal conditions. Here, we reported the development of cellulose nanocomposite thin films in which TOCNCs were used to reinforce a soft polymer matrix such as CMC. The resulting films took advantage of the hydrogen bonds established between the matrix and the nanofillers, which provided an efficient stress transfer mechanism, allowing to more than double the strength and the stiffness, as well as the toughness of the nanocomposite films with respect to pure CMC films while preserving its deformation capability. A further enhancement of strength and Young's modulus was shown to be achievable by adding multivalent metal ions, such as Fe^{3+}, with limited impact on the strain at failure. We have demonstrated the importance of metal−ligand coordination bonds in promoting cross-linking between the CMC and CNC chains, resulting in improved mechanical properties of the films and, at the same time, introducing redox- and photoresponsive properties to the film thanks to the presence of the Fe^{3+} ions. The introduction of Fe^{3+} coordination cross-linkers represents a significant advancement in cellulose-based nanocomposite films, enabling a broader range of applications in various fields ranging from decontamination to catalysis. Finally, the developed cellulose nanocomposite thin films showed stable mechanical behavior when subjected to cyclic tensile tests. This aspect makes them suitable for adoption in advanced realistic device applications, such as thin membranes for environmental-related processes and actuators for soft robotics.

ASSOCIATED CONTENT

Supporting Information

The Supporting Information is available free of charge at https://pubs.acs.org/doi/10.1021/acsanm.3c02946.

Optical images of the developed cellulose-based thin films; XPS spectra; cross-section SEM images at higher magnification; apparatus for mechanical characterization; stress−strain curves; hysteresis curves of a CMC/TOCNC sample; stress−strain curves of CMC/TOCNC and (CMC/TOCNC)Fe-low films after cyclic tests (PDF)

AUTHOR INFORMATION

Corresponding Author

Maria F. Pantano − *Department of Civil, Environmental and Mechanical Engineering, University of Trento, 38123 Trento, Italy;* orcid.org/0000-0001-5415-920X; Email: maria.pantano@unitn.it

Authors

Elena Missale − *Department of Civil, Environmental and Mechanical Engineering, University of Trento, 38123 Trento, Italy*

Devid Maniglio − *BIOtech Center for Biomedical Technologies, Department of Industrial Engineering, University of Trento, Trento 38123, Italy; European Institute of Excellence on Tissue Engineering and Regenerative Medicine Unit, Trento 38123, Italy;* orcid.org/0000-0002-1653-861X

Giorgio Speranza − *Centre for Materials and Microsystems, Fondazione Bruno Kessler, 38123 Trento, Italy; Department of Industrial Engineering, University of Trento, 38123 Trento, Italy;* orcid.org/0000-0003-1478-0995

Marco Frasconi − *Department of Chemical Sciences, University of Padova, 35131 Padova, Italy;* orcid.org/0000-0003-2010-175X

Complete contact information is available at: https://pubs.acs.org/10.1021/acsanm.3c02946

Notes

The authors declare no competing financial interest.

ACKNOWLEDGMENTS

The authors thank Mr. Alessandro Lugnani for his support in the development of the microscopy experimental setup. M.F.P. acknowledges the support of Fondazione CARITRO, Cassa di Risparmio di Trento e Rovereto and Fondazione VRT, Fondazione per la Valorizzazione della Ricerca Trentina, 3° Bando Impact Innovation 2021. M.F. thanks the University of Padova for funding support with the 2019 STARS grant program "SensCo".

REFERENCES

(1) Olivetti, E. A.; Cullen, J. M. Toward a Sustainable Materials System. *Science* **2018**, *360* (6396), 1396−1398.

(2) Irimia-Vladu, M. "Green" Electronics: Biodegradable and Biocompatible Materials and Devices for Sustainable Future. *Chem. Soc. Rev.* **2014**, *43* (2), 588−610.

(3) Lan, L.; Ping, J.; Xiong, J.; Ying, Y. Sustainable Natural Bio-Origin Materials for Future Flexible Devices. *Adv. Sci.* **2022**, *9*, No. 2200560.

(4) Li, T.; Chen, C.; Brozena, A. H.; Zhu, J. Y.; Xu, L.; Driemeier, C.; Dai, J.; Rojas, O. J.; Isogai, A.; Wågberg, L.; Hu, L. Developing Fibrillated Cellulose as a Sustainable Technological Material. *Nature* **2021**, *590* (7844), 47−56.

(5) Carpenter, A. W.; De Lannoy, C. F.; Wiesner, M. R. Cellulose Nanomaterials in Water Treatment Technologies. *Environ. Sci. Technol.* **2015**, *49* (9), 5277−5287.

(6) Wang, J.; Gardner, D. J.; Stark, N. M.; Bousfield, D. W.; Tajvidi, M.; Cai, Z. Moisture and Oxygen Barrier Properties of Cellulose Nanomaterial-Based Films. *ACS Sustain. Chem. Eng.* **2018**, *6* (1), 49−70.
(7) Cherian, R. M.; Tharayil, A.; Varghese, R. T.; Antony, T.; Kargarzadeh, H.; Chirayil, C. J.; Thomas, S. A Review on the Emerging Applications of Nano-Cellulose as Advanced Coatings. *Carbohydr. Polym.* **2022**, *282*, No. 119123.
(8) Jung, Y. H.; Chang, T. H.; Zhang, H.; Yao, C.; Zheng, Q.; Yang, V. W.; Mi, H.; Kim, M.; Cho, S. J.; Park, D. W.; Jiang, H.; Lee, J.; Qiu, Y.; Zhou, W.; Cai, Z.; Gong, S.; Ma, Z. High-Performance Green Flexible Electronics Based on Biodegradable Cellulose Nanofibril Paper. *Nat. Commun.* **2015**, *6*, 7170.
(9) Zhao, D.; Zhu, Y.; Cheng, W.; Chen, W.; Wu, Y.; Yu, H. Cellulose-Based Flexible Functional Materials for Emerging Intelligent Electronics. *Adv. Mater.* **2021**, *33*, No. 2000619.
(10) Seddiqi, H.; Oliaei, E.; Honarkar, H.; Jin, J.; Geonzon, L. C.; Bacabac, R. G.; Klein-Nulend, J. Cellulose and Its Derivatives: Towards Biomedical Applications. *Cellulose* **2021**, *28* (4), 1893−1931.
(11) Du, H.; Liu, W.; Zhang, M.; Si, C.; Zhang, X.; Li, B. Cellulose Nanocrystals and Cellulose Nanofibrils Based Hydrogels for Biomedical Applications. *Carbohydr. Polym.* **2019**, *209*, 130−144.
(12) Wang, X.; Yao, C.; Wang, F.; Li, Z. Cellulose-Based Nanomaterials for Energy Applications. *Small* **2017**, *13*, No. 1702240.
(13) Liu, S.; Low, Z. X.; Xie, Z.; Wang, H. TEMPO-Oxidized Cellulose Nanofibers: A Renewable Nanomaterial for Environmental and Energy Applications. *Adv. Mater. Technol.* **2021**, *6* (7), No. 2001180.
(14) Abitbol, T.; Kam, D.; Levi-Kalisman, Y.; Gray, D. G.; Shoseyov, O. Surface Charge Influence on the Phase Separation and Viscosity of Cellulose Nanocrystals. *Langmuir* **2018**, *34* (13), 3925−3933.
(15) Heise, K.; Kontturi, E.; Allahverdiyeva, Y.; Tammelin, T.; Linder, M. B.; Nonappa; Ikkala, O. Nanocellulose: Recent Fundamental Advances and Emerging Biological and Biomimicking Applications. *Adv. Mater.* **2021**, *33* (3), No. 2004349.
(16) Ghasemlou, M.; Daver, F.; Ivanova, E. P.; Murdoch, B. J.; Adhikari, B. Use of Synergistic Interactions to Fabricate Transparent and Mechanically Robust Nanohybrids Based on Starch, Non-Isocyanate Polyurethanes, and Cellulose Nanocrystals. *ACS Appl. Mater. Interfaces* **2020**, *12* (42), 47865−47878.
(17) Hopcroft, M. A.; Nix, W. D.; Kenny, T. W. What Is the Young's Modulus of Silicon? *J. Microelectromechanical Syst.* **2010**, *19* (2), 229−238.
(18) Liu, H. K.; Pan, C. H.; Liu, P. P. Dimension Effect on Mechanical Behavior of Silicon Micro-Cantilever Beams. *Measurement* **2008**, *41* (8), 885−895.
(19) Saha, P.; Ansari, N.; Kitchens, C. L.; Ashurst, W. R.; Davis, V. A. Microelectromechanical Systems from Aligned Cellulose Nanocrystal Films. *ACS Appl. Mater. Interfaces* **2018**, *10* (28), 24116−24123.
(20) Reid, L.; Hamad, W. Y. Electro-Osmotic Actuators from Cellulose Nanocrystals and Nanocomposite Hydrogels. *ACS Appl. Polym. Mater.* **2022**, *4* (1), 598−606.
(21) Abdul Khalil, H. P. S.; Bhat, A. H.; Ireana Yusra, A. F. Green Composites from Sustainable Cellulose Nanofibrils: A Review. *Carbohydr. Polym.* **2012**, *87* (2), 963−979.
(22) Hoeger, I.; Rojas, O. J.; Efimenko, K.; Velev, O. D.; Kelley, S. S. Ultrathin Film Coatings of Aligned Cellulose Nanocrystals from a Convective-Shear Assembly System and Their Surface Mechanical Properties. *Soft Matter* **2011**, *7* (5), 1957−1967.
(23) Chen, Z.; Hu, Y.; Shi, G.; Zhuo, H.; Ali, M. A.; Jamróz, E.; Zhang, H.; Zhong, L.; Peng, X. Advanced Flexible Materials from Nanocellulose. *Adv. Funct. Mater.* **2023**, *33*, No. 2214245.
(24) Abraham, E.; Kam, D.; Nevo, Y.; Slattegard, R.; Rivkin, A.; Lapidot, S.; Shoseyov, O. Highly Modified Cellulose Nanocrystals and Formation of Epoxy-Nanocrystalline Cellulose (CNC) Nanocomposites. *ACS Appl. Mater. Interfaces* **2016**, *8* (41), 28086−28095.
(25) Adstedt, K.; Popenov, E. A.; Pierce, K. J.; Xiong, R.; Geryak, R.; Cherpak, V.; Nepal, D.; Bunning, T. J.; Tsukruk, V. V. Chiral Cellulose Nanocrystals with Intercalated Amorphous Polysaccharides for Controlled Iridescence and Enhanced Mechanics. *Adv. Funct. Mater.* **2020**, *30* (49), No. 2003597.
(26) Gabrielli, V.; Missale, E.; Cattelan, M.; Pantano, M. F.; Frasconi, M. Supramolecular Modulation of the Mechanical Properties of Amino Acid-Functionalized Cellulose Nanocrystal Films. *Mater. Today Chem.* **2022**, *24*, No. 100886.
(27) Akhlaghi, S. P.; Berry, R. C.; Tam, K. C. Surface Modification of Cellulose Nanocrystal with Chitosan Oligosaccharide for Drug Delivery Applications. *Cellulose* **2013**, *20* (4), 1747−1764.
(28) Nori, U. M.; Gomez-Maldonado, D.; Saha, P.; Ashurst, W. R.; Peresin, M. S.; Davis, V. A. Antibody Immobilization on Sulfated Cellulose Nanocrystals. *Biomacromolecules* **2023**, *24*, 1103−1110.
(29) Missale, E.; Frasconi, M.; Pantano, M. F. Ultrathin Organic Membranes: Can They Sustain the Quest for Mechanically Robust Device Applications? *iScience* **2023**, *26* (2), No. 105924.
(30) Kono, H. Characterization and Properties of Carboxymethyl Cellulose Hydrogels Crosslinked by Polyethylene Glycol. *Carbohydr. Polym.* **2014**, *106* (1), 84−93.
(31) Oun, A. A.; Rhim, J. W. Isolation of Cellulose Nanocrystals from Grain Straws and Their Use for the Preparation of Carboxymethyl Cellulose-Based Nanocomposite Films. *Carbohydr. Polym.* **2016**, *150*, 187−200.
(32) Baretta, R.; Gabrielli, V.; Frasconi, M. Nanozyme−Cellulose Hydrogel Composites Enabling Cascade Catalysis for the Colorimetric Detection of Glucose. *ACS Appl. Nano Mater.* **2022**, *5*, 13845−13853.
(33) Tavares, K. M.; Campos, A. de; Luchesi, B. R.; Resende, A. A.; Oliveira, J. E. de; Marconcini, J. M. Effect of Carboxymethyl Cellulose Concentration on Mechanical and Water Vapor Barrier Properties of Corn Starch Films. *Carbohydr. Polym.* **2020**, *246*, No. 116521.
(34) Fernández-Santos, J.; Valls, C.; Cusola, O.; Roncero, M. B. Composites of Cellulose Nanocrystals in Combination with Either Cellulose Nanofibril or Carboxymethylcellulose as Functional Packaging Films. *Int. J. Biol. Macromol.* **2022**, *211*, 218−229.
(35) Wang, B.; Torres-Rendon, J. G.; Yu, J.; Zhang, Y.; Walther, A. Aligned Bioinspired Cellulose Nanocrystal-Based Nanocomposites with Synergetic Mechanical Properties and Improved Hygromechanical Performance. *ACS Appl. Mater. Interfaces* **2015**, *7* (8), 4595−4607.
(36) El Miri, N.; Abdelouahdi, K.; Barakat, A.; Zahouily, M.; Fihri, A.; Solhy, A.; El Achaby, M. Bio-Nanocomposite Films Reinforced with Cellulose Nanocrystals: Rheology of Film-Forming Solutions, Transparency, Water Vapor Barrier and Tensile Properties of Films. *Carbohydr. Polym.* **2015**, *129*, 156−167.
(37) Oun, A. A.; Rhim, J. W. Characterization of Carboxymethyl Cellulose-Based Nanocomposite Films Reinforced with Oxidized Nanocellulose Isolated Using Ammonium Persulfate Method. *Carbohydr. Polym.* **2017**, *174*, 484−492.
(38) Liu, X.; Jiang, Y.; Wei, Y.; Wei, X. Strengthening and Toughening Mechanisms Induced by Metal Ion Cross-Linking in Wet-Drawn Bacterial Cellulose Films. *Mater. Des.* **2022**, *224*, No. 111431.
(39) Gabrielli, V.; Baretta, R.; Pilot, R.; Ferrarini, A.; Frasconi, M. Insights into the Gelation Mechanism of Metal-Coordinated Hydrogels by Paramagnetic NMR Spectroscopy and Molecular Dynamics. *Macromolecules* **2022**, *55* (2), 450−461.
(40) Gabrielli, V.; Ferrarini, A.; Frasconi, M. A Study across Scales to Unveil Microstructuralregimes in the Multivalent Metal Driven Self-Assembly of Cellulose Nanocrystals. *Nanoscale* **2023**, *15*, 13384.
(41) Wang, D.; Yang, J.; Yang, H.; Zhao, P.; Shi, Z. Fe-Complex Modified Cellulose Acetate Composite Membrane with Excellent Photo-Fenton Catalytic Activity. *Carbohydr. Polym.* **2022**, *296*, No. 119960.
(42) Speranza, G.; Canteri, R. RxpsG a New Open Project for Photoelectron and Electron Spectroscopy Data Processing. *SoftwareX* **2019**, *10*, No. 100282.

https://doi.org/10.1021/acsanm.3c02946
ACS Appl. Nano Mater. XXXX, XXX, XXX−XXX

(43) Nečas, D.; Klapetek, P. Gwyddion: An Open-Source Software for SPM Data Analysis. *Cent. Eur. J. Phys.* **2012**, *10* (1), 181−188.
(44) Pantano, M. F.; Speranza, G.; Galiotis, C.; Pugno, N. A Mechanical System for Tensile Testing of Supported Films at the Nanoscale. *Nanotechnology* **2018**, *29* (39), No. 395707.
(45) Pantano, M. F.; Missale, E.; Gazzato, L.; Pilot, R.; Sedona, F.; Speranza, G.; Frasconi, M. Large Freestanding 2D Covalent Organic Framework Nano Films Exhibiting High Strength and Stiffness. *Mater. Today Chem.* **2022**, *26*, No. 101007.
(46) Foster, E.; Moon, R.; Agarwal, U.; Bortner, M.; Bras, J.; Camarero-Espinosa, S.; Chan, K.; Clift, M.; Cranston, E.; Eichhorn, S.; Fox, D.; Hamad, W.; Heux, L.; et al. Current Characterization Methods for Cellulose Nanomaterials. *Chem. Soc. Rev.* **2018**, *47* (8), 2609−2679.
(47) Oun, A. A.; Rhim, J. W. Preparation and Characterization of Sodium Carboxymethyl Cellulose/Cotton Linter Cellulose Nanofibril Composite Films. *Carbohydr. Polym.* **2015**, *127*, 101−109.
(48) Barazzouk, S.; Daneault, C. Spectroscopic Characterization of Oxidized Nanocellulose Grafted with Fluorescent Amino Acids. *Cellulose* **2011**, *18* (3), 643−653.
(49) Xu, Y.; Atrens, A. D.; Stokes, J. R. Rheology and Microstructure of Aqueous Suspensions of Nanocrystalline Cellulose Rods. *J. Colloid Interface Sci.* **2017**, *496*, 130−140.
(50) Berardo, A.; Pantano, M. F.; Pugno, N. M. An Insight into the Toughness Modulus Enhancement of Highperformance Knotted Microfibers through the Correspondence Analysis. *Eng. Res. Express* **2021**, 3 (2), No. 025010.
(51) Wegst, U. G. K.; Bai, H.; Saiz, E.; Tomsia, A. P.; Ritchie, R. O. Bioinspired Structural Materials. *Nat. Mater.* **2015**, *14* (1), 23−36.
(52) Yang, X.; Jungstedt, E.; Reid, M. S.; Berglund, L. A. Polymer Films from Cellulose Nanofibrils - Effects from Interfibrillar Interphase on Mechanical Behavior. *Macromolecules* **2021**, *54* (9), 4443−4452.
(53) Amini, M.; Kamkar, M.; Ahmadijokani, F.; Ghaderi, S.; Rojas, O. J.; Hosseini, H.; Arjmand, M. Mapping 3D Printability of Ionically Cross-Linked Cellulose Nanocrystal Inks: Architecting from Nano- to Macroscale Structures. *Biomacromolecules* **2023**, *24* (2), 775−788.
(54) Mittal, N.; Benselfelt, T.; Ansari, F.; Gordeyeva, K.; Roth, S. V.; Wagberg, L.; Soderberg, L. D. Ion-Specific Assembly of Strong Tough and Stiff Biofibers. *Angew. Chem.* **2019**, *131*, 18735−18742.
(55) Benselfelt, T.; Nordenström, M.; Lindström, S. B.; Wågberg, L. Explaining the Exceptional Wet Integrity of Transparent Cellulose Nanofibril Films in the Presence of Multivalent Ions—Suitable Substrates for Biointerfaces. *Adv. Mater. Interfaces* **2019**, *6* (13), No. 1900333.

https://doi.org/10.1021/acsanm.3c02946
ACS Appl. Nano Mater. XXXX, XXX, XXX−XXX